

## Note: Guaranteed collocated multimode control of an atomic force microscope cantilever using on-chip piezoelectric actuation and sensing

Michael G. Ruppert and , and Yuen K. Yong

Citation: *Review of Scientific Instruments* **88**, 086109 (2017); doi: 10.1063/1.4990451

View online: <http://dx.doi.org/10.1063/1.4990451>

View Table of Contents: <http://aip.scitation.org/toc/rsi/88/8>

Published by the *American Institute of Physics*

---

---



## Note: Guaranteed collocated multimode control of an atomic force microscope cantilever using on-chip piezoelectric actuation and sensing

Michael G. Ruppert<sup>a)</sup> and Yuen K. Yong<sup>b)</sup>

*The University of Newcastle, University Drive, Callaghan, NSW 2308, Australia*

(Received 15 June 2017; accepted 30 July 2017; published online 15 August 2017)

The quality (Q) factor is an important parameter of the resonance of the microcantilever as it determines both imaging bandwidth and force sensitivity. The ability to control the Q factor of multiple modes is believed to be of great benefit for atomic force microscopy techniques involving multiple eigenmodes. In this paper, we propose a novel cantilever design employing multiple piezoelectric transducers which are used for separated actuation and sensing, leading to guaranteed collocation of the first eight eigenmodes up to 3 MHz. The design minimizes the feedthrough usually observed with these systems by incorporating a guard trace on the cantilever chip. As a result, a multimode Q controller is demonstrated to be able to modify the quality factor of the first two eigenmodes over up to four orders of magnitude without sacrificing robust stability. *Published by AIP Publishing.* [<http://dx.doi.org/10.1063/1.4990451>]

Dynamic Atomic Force Microscopy (AFM) operating modes can map the surface topography and material composition of specimen with nanometer spatial resolution by scanning a sharp tip at the end of an actively driven microcantilever over the surface of a sample.<sup>1,2</sup>

Conventionally, the cantilever is used “as is,” i.e., the eigenmodes in terms of their quality (Q) factors are left uncontrolled. However, the Q factor directly affects the imaging bandwidth as the transient response of the *i*-th mode decays exponentially with the time constant  $\tau_i = 2Q_i/\omega_i$ .<sup>3</sup> Further, the average tip-sample force  $\bar{F}_{ts}$  and the average power dissipation  $\bar{P}_{ts}$  are also a function of the Q factor of the active eigenmode.<sup>4,5</sup>

Originally introduced to reduce the quality factor of the fundamental mode of the cantilever,<sup>6</sup> active Q control can increase the scan speed by reducing the transient response of the cantilever.<sup>7</sup> On the other hand, actively increasing the quality factor was shown to be beneficial for imaging sensitivity,<sup>8</sup> particularly when imaging in liquids.<sup>9</sup>

However, the common method for active modification of the cantilever Q factor is based on the time-delay method,<sup>10</sup> which is an easy method to implement solution but comes with a number of disadvantages. These include the restriction to controlling the fundamental mode, non-robust stability properties,<sup>11</sup> and limited damping performance.<sup>12</sup> These limitations can be overcome by using model-based resonant controllers although these require integrated actuation to avoid the additional dynamics caused by the stack actuator.<sup>13</sup> With controllers of this type, it was shown that multiple eigenmodes can be controlled simultaneously which enables imaging on higher eigenmodes<sup>14</sup> and optimizing the material contrast in bimodal AFM.<sup>15</sup>

The aforementioned Q control methods all rely on the feedback from the optical beam deflection sensor, as it remains the most widely used approach to detect the cantilever oscillations. However, the uncertainty in the position of the laser spot on the cantilever usually leads to a non-collocated actuator-sensor system,<sup>14</sup> reducing the stability margins for Q control. This problem can be overcome by integrated sensing methods enabled by microelectromechanical system (MEMS) fabrication processes such as piezoelectric sensing,<sup>16</sup> which were shown to provide multi-mode displacement estimates.<sup>17,18</sup> The actuator-sensor configuration proposed in this work yields a guaranteed collocated system, a property which is highly

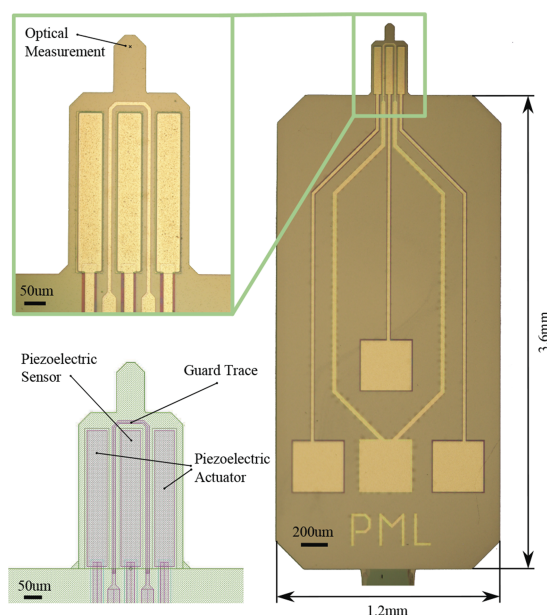


FIG. 1. Design schematic and photo of fabricated piezoelectric MEMS cantilever with integrated actuation and sensing.

<sup>a)</sup>Electronic mail: Michael.Ruppert@newcastle.edu.au

<sup>b)</sup>Electronic mail: Yuenkuan.Yong@newcastle.edu.au

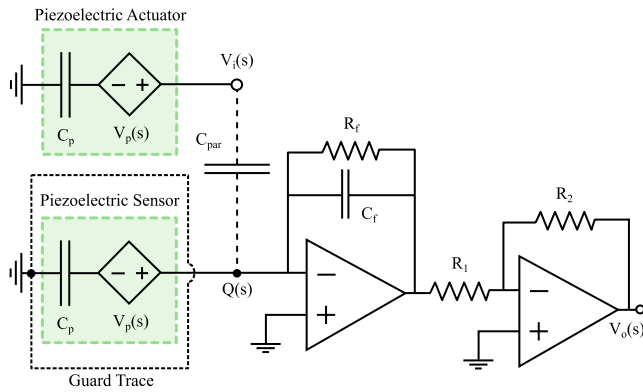


FIG. 2. Implementation of the piezoelectric instrumentation.

desirable for vibration control as it results in guaranteed robust stability of the closed loop.<sup>19</sup>

The cantilever geometry chosen for this work is a stepped rectangular design as shown in Fig. 1, which has the benefit of closely spaced higher eigenmodes.<sup>20</sup> The cantilever consists of a wider section with dimensions of  $360 \mu\text{m} \times 390 \mu\text{m}$  and a smaller section with dimensions of  $70 \mu\text{m} \times 125 \mu\text{m}$ .

Three laterally symmetric piezoelectric patches are placed on the cantilever, the outer two patches form the actuators and the inner patch serves as the sensor. The equal longitudinal placement of the three transducers guarantees the collocation property of the actuator-sensor system. In order to minimize the feedthrough from the actuators to the sensing patch via the common silicon substrate,<sup>21</sup> a metal guard trace is incorporated which completely surrounds the piezoelectric sensor.

The fabricated design (MEMSCAP, PiezoMUMPs) features a  $10 \mu\text{m}$  silicon device layer, a  $0.5 \mu\text{m}$  aluminum nitride piezoelectric layer, and chrome/aluminum metal traces<sup>22</sup> and is shown in Fig. 1. The schematic of the piezoelectric instrumentation is shown in Fig. 2. The outer piezoelectric patches (drawn as one piezoelectric actuator) are driven by the input voltage  $V_i(s)$ . A charge-mode amplifier is used as the first stage, which amplifies the charge generated by the strain-dependent piezoelectric voltage  $V_p(s)$  on the piezoelectric capacitance  $C_p$ . The benefit of this circuit is that the high-frequency sensor gain depends only on the feedback capacitance  $C_f$  and is independent of the input capacitance at the op-amp. The circuit forms a high-pass filter from piezoelectric charge to first stage output voltage

$$H(s) = \frac{-R_f s}{R_f C_f s + 1}, \quad (1)$$

where the high-frequency charge-to-voltage gain is  $1/C_f$  and the corner frequency is given by  $f_c = (2\pi R_f C_f)^{-1}$ . With the chosen circuit values of  $R_f = 1 \text{ M}\Omega$  and  $C_f = 20 \text{ pF}$ , the resulting charge-to-voltage gain is 214 dB and the cut-off frequency is 8 kHz which is adequately lower than the first resonance mode at 62 kHz. An inverting gain stage is added after the charge-mode amplifier for additional gain and accommodating for the negation.

The transfer function from actuator voltage  $V_i(s)$  to cantilever deflection  $D(s)$  of the first  $n$  flexural modes can be

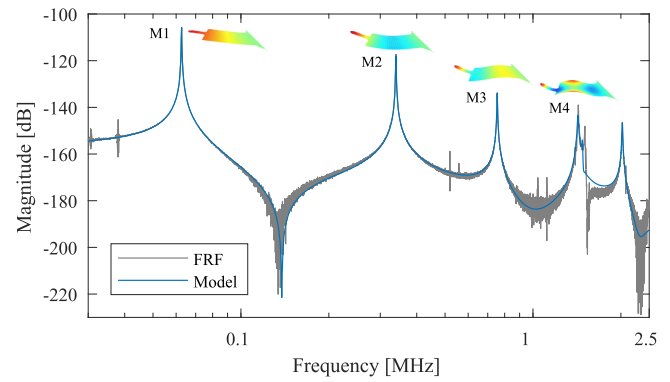


FIG. 3. Frequency response function (FRF) and identified model (2) from actuation voltage to tip displacement (measurement location see Fig. 1) and mode shapes measured with a laser-Doppler vibrometer.

described by a sum of second order modes,<sup>23</sup>

$$G_{dv}(s) = \frac{D(s)}{V_i(s)} = \sum_{i=1}^n \frac{\alpha_i \omega_i^2}{s^2 + \frac{\omega_i}{Q_i} s + \omega_i^2}, \quad \alpha_i \in \mathbb{R}, \quad (2)$$

where each mode is associated with a specific vibrational mode shape, quality factor  $Q_i$ , natural frequency  $\omega_i$ , and gain  $\alpha_i$ . Note that  $\alpha_i \in \mathbb{R}$  does not guarantee that  $G_{dv}(s)$  is collocated. Similarly, when a piezoelectric transducer is subjected to mechanical strain, it produces a charge which for the instrumentation chosen here is given by

$$Q(s) = -C_p V_p(s) + D V_i(s), \quad (3)$$

where  $D = C_{\text{par}}$  is the parasitic capacitance between the actuator and the sensor causing a residual amount of feedthrough charge with opposite sign to the motional charge. Within the bandwidth of the read-out circuit, the resulting transfer function from actuator voltage  $V_i(s)$  to sensor output  $V_o(s)$  is hence described by

$$G(s) = \frac{V_o(s)}{V_i(s)} = -C_p G_{vv}(s) + D, \quad (4)$$

where

$$G_{vv}(s) = \frac{V_p(s)}{V_i(s)} = \sum_{i=1}^n \frac{\beta_i \omega_i^2}{s^2 + \frac{\omega_i}{Q_i} s + \omega_i^2}, \quad \beta_i > 0, \quad (5)$$

is the collocated transfer function from actuator voltage to piezoelectric voltage.<sup>23</sup> Given that  $G_{vv}(s)$  is guaranteed collocated ( $\beta_i > 0$ ), the overall transfer function  $-G(s)$  is also collocated for all  $D \in \mathbb{R}$ .

To control  $m$  modes of the cantilever, the positive position feedback controller (PPF)<sup>24</sup> of the form

$$K(s) = \sum_{i=1}^m \frac{\gamma_{c,i}}{s^2 + 2\zeta_{c,i}\omega_{c,i}s + \omega_{c,i}^2}, \quad (6)$$

TABLE I. Modal parameters of the first four modes of the cantilever.

	Mode 1	Mode 2	Mode 3	Mode 4
$f_i$ (kHz)	62.6	339.5	754.5	1430.3
$Q_i$	411	490	320	239
$\alpha_i$ (nm/V)	12.7	3.41	-0.64	0.48

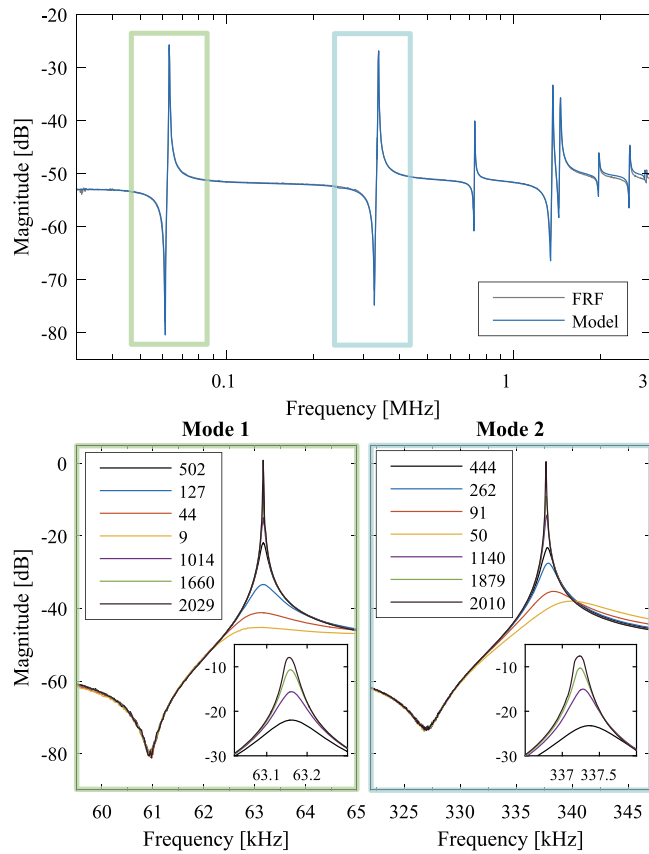


FIG. 4. Top: Open-loop frequency response and model (4) of the piezoelectric sensor. Bottom: Open-loop (black) and closed-loop frequency responses for various controller gains to lower and increase the Q factor of the first and second eigenmodes. The achieved Q factors are stated in the legend.

with  $\gamma_{c,i}$ ,  $\zeta_{c,i}$ , and  $\omega_{c,i}$  being the positive tunable controller parameters is used. Controllers of this type used in positive feedback with a collocated system inherit robust closed-loop stability originating from the negative imaginary property of the plant and the controller if the loop gain is less than one at low frequencies.<sup>19</sup>

A laser-Doppler vibrometer (Polytec MSA-100-3D) is used to determine the tip displacement frequency responses and corresponding mode shapes of the cantilever by performing a full modal scan using a periodic chirp excitation signal. The frequency response is shown in Fig. 3 along with the identified model (2) and the mode shapes of the first four flexural modes. From the mode shapes and the pole/zero pattern of the frequency response, it can be clearly observed that the tip displacement is not collocated with the actuation beyond the second mode. The identified parameters of (2) are stated in Table I.

The measured open-loop frequency response of the piezoelectric actuator-sensor system is shown in the top row of Fig. 4 along with the identified model (4). In contrast to Fig. 3, the interlacing poles and zeros are clearly visible up to a frequency

of around 3 MHz, showing the collocated characteristic of the proposed design.

Due to its high achievable controller bandwidth of 400 kHz, a field-programmable analog array (FPAA) (Anadigm AN221E04) was chosen for the implementation of the multimode Q controller. The controller was set to adjust the Q factor of the first and second eigenmodes by running a pole placement optimization design routine.<sup>14</sup> The resulting closed loop formed by  $-G(s)$  and  $K(s)$  remains stable over a large range of positive parameter values due to the collocated system structure. Therefore, as can be seen from the bottom row in Fig. 4, the Q factors of the first and second modes can be adjusted over a range of four and three orders of magnitude, respectively. On the first mode, an initial Q factor of 502 can be lowered to 9 and increased to over 2000. On the second mode, an initial Q factor of 444 can be lowered to 50 and increased to over 2000. The difference in the dynamic range for controlling the second mode Q factor can be attributed to the controller reaching the bandwidth limitation of 400 kHz.

<sup>1</sup>F. J. Giessibl, *Science* **267**, 68 (1995).

<sup>2</sup>E. T. Herruzo, A. P. Perrino, and R. Garcia, *Nat. Commun.* **5**, 3126 (2014).

<sup>3</sup>T. Ando, T. Uchihashi, and T. Fukuma, *Prog. Surf. Sci.* **83**, 337 (2008).

<sup>4</sup>A. S. Paulo and R. Garcia, *Phys. Rev. B* **64**, 193411 (2001).

<sup>5</sup>B. Anczykowski, B. Gotsmann, H. Fuchs, J. P. Cleveland, and V. Elings, *Appl. Surf. Sci.* **140**, 376 (1999).

<sup>6</sup>J. Mertz, O. Marti, and J. Mlynek, *Appl. Phys. Lett.* **62**, 2344 (1993).

<sup>7</sup>T. Sulchek, R. Hsieh, J. D. Adams, G. G. Yaralioglu, S. C. Minne, and C. F. Quate, *Appl. Phys. Lett.* **76**(11), 1473 (2000).

<sup>8</sup>A. Humphris, A. Round, and M. Miles, *Surf. Sci.* **491**, 468 (2001).

<sup>9</sup>J. Tamayo, A. D. L. Humphris, and M. J. Miles, *Appl. Phys. Lett.* **77**, 582 (2000).

<sup>10</sup>T. R. Rodriguez and R. Garcia, *Appl. Phys. Lett.* **82**, 4821 (2003).

<sup>11</sup>R. W. Stark, in *5th IEEE Conference on Nanotechnology* (IEEE, 2005), Vol. 1, pp. 259–262.

<sup>12</sup>H. Hölscher, D. Ebeling, and U. D. Schwarz, *J. Appl. Phys.* **99**, 084311 (2006).

<sup>13</sup>M. W. Fairbairn and S. O. R. Moheimani, *Rev. Sci. Instrum.* **83**, 083708 (2012).

<sup>14</sup>M. G. Ruppert and S. O. R. Moheimani, *IEEE Trans. Control Syst. Technol.* **24**, 1149 (2016).

<sup>15</sup>M. G. Ruppert and S. O. R. Moheimani, in *Proceedings of ASME International Design Engineering Technical Conference and the Computer and Information in Engineering Conference (IDETC/CIE)* (ASME, Boston, Massachusetts, USA, 2015), Vol. 4, p. V004T09A009.

<sup>16</sup>T. Itoh and T. Suga, *Nanotechnology* **4**, 218 (1993).

<sup>17</sup>M. G. Ruppert and S. O. R. Moheimani, *Beilstein J. Nanotechnol.* **7**, 284 (2016).

<sup>18</sup>S. I. Moore, M. G. Ruppert, and Y. K. Yong, *Beilstein J. Nanotechnol.* **8**, 358 (2017).

<sup>19</sup>I. Petersen and A. Lanzon, *IEEE Control Syst. Mag.* **30**, 54 (2010).

<sup>20</sup>S. Sadewasser, G. Villanueva, and J. A. Plaza, *Rev. Sci. Instrum.* **77**, 073703 (2006).

<sup>21</sup>M. G. Ruppert and S. O. R. Moheimani, *Rev. Sci. Instrum.* **84**, 125006 (2013).

<sup>22</sup>A. Cowen, G. Hames, K. Glukh, and B. Hardy, *PiezoMUMPs Design Handbook*, 1st ed. (MEMSCAP Inc., 2014).

<sup>23</sup>S. O. R. Moheimani and A. J. Fleming, *Piezoelectric Transducers for Vibration Control and Damping* (Springer-Verlag London Limited, 2006).

<sup>24</sup>J. Fanson and T. K. Caughey, *AIAA J.* **28**, 717 (1990).